MODELING RESIDUAL STRESSES IN OFFSHORE CHAIN LINKS USING FINITE ELEMENT METHOD

Pedro Manuel Calas Lopes Pacheco
Paulo Pedro Kenedi
Jorge Carlos Ferreira Jorge
Hugo Gama dos Santos
CEFET/RJ - Department of Mechanical Engineering
20.271.110 - Rio de Janeiro - RJ - Brazil
E-mail: calas@cefet-rj.br, pkenedi@cefet-rj.br, jorge@cefet-rj.br, hugogs@ig.com.br

Marcelo Amorim Savi
UFRJ/COPPE - Department of Mechanical Engineering
21.945.970 – Rio de Janeiro – RJ – Brazil
Cx. Postal 68.503
E-mail: savi@ufrj.br

Augusto Marcos Coelho de Paiva
PETROBRAS – E&P / SC /USSUB / Ancoragem
27913-350 - Macaé / RJ - Brazil
E-mail: amarcoelho@ petrobras.com.br

Abstract. The continuous expansion of deepwater petroleum activities has resulted in an increasing attention to the design of mooring systems. The failure of a single element in a mooring line of an offshore oil exploitation platform can produce incalculable environment damage as well as human and material losses. Production offshore units have a relative long operational life (about 20 years), during which are subjected to the ocean adverse environment loading produced by a combination of wind, waves and sea currents. This complex loading history can promote the nucleation and propagation of cracks in components of mooring lines and it is well known that the presence of defects in elements of such lines means a critical situation that can lead to catastrophic failures. Residual stresses have a preponderant effect on the structural integrity of a mechanical component subjected to such loadings. Offshore mooring line components like chain links enter in operation with a residual stress field created by the proof test dictated by offshore standards. However, the traditional design of such mechanical components does not consider residual stresses. For this reason, it is fundamental to develop new and more precise methodologies assessing structural integrity of mooring components. In this work, numerical simulations employing a tridimensional elastoplastic finite element model are used to estimate residual stress distributions in studless chain links before operation. Moreover, a bidimensional elastoplastic finite element model with contact is used to study the contact region between two chain links. Results indicate that residual stresses are dependent on the material condition and significantly modifies the stress distribution in the component. A simplified analysis of the effect of the residual stresses on the fatigue life based on S-N curve is presented. The analysis shows that the residual stress has a preponderant effect on structural integrity of chain links. Results also show the importance of modeling the contact phenomena between the chain links.

Keywords. Chain link, Residual Stresses, Modeling, Finite Element, Contact, Elastoplasticity.

1. Introduction

Deepwater petroleum activities are in continuous expansion and the design of mooring systems has been gaining increased attention (Chaplin *et al.*, 2000; Papazoglou 1991; Paiva, 2000). Production offshore units have a relative long operational life (about 20 years), during which are subjected to ocean adverse environment loading produced by the combination of wind, waves and sea currents. This complex loading history can promote the nucleation and propagation of cracks in mooring line components and it is well known that the presence of defects in elements of such lines establishes a critical situation that can lead to catastrophic failures. The failure of a single element in a mooring line of an offshore oil exploitation platform can produce incalculable environment damage as well as human and material losses.

Offshore mooring line components like chain links must be submitted to a mandatory proof test, dictated by offshore standards, where loads higher than the operational load are applied to the mechanical component, resulting in high levels of residual stresses. Traditional design and inspection methodologies are very conservative (API, 1995; Hasson and Crowe, 1988; Stern and Weatcroft, 1978). In order to permit the use of simple design methodologies, effects like the presence of residual stress fields promoted by fabrication processes are not considered in the analysis. Meanwhile, it is well known that residual stress plays a preponderant part on the structural integrity of a mechanical component, especially in nucleation and propagation of cracks (SAE, 1988; Almer *et al.*, 2000, Webster and Ezeilo, 2001). Tensile residual stresses can be especially dangerous since fatigue cracks usually propagate by tensile stress field. In the presence of tensile stresses promoted by the operational loading conditions, both stresses are added resulting in much higher tensile stress levels than the ones predicted by the design process. On the other way, compressive residual stresses can be beneficial because, during operation, they are subtracted from tensile stresses generated by the operational loading. Therefore, a detailed knowledge of the residual stress field is required for an accurate assessment of mechanical component integrity (Pacheco *et al.*, 2002; Shoup *et al.*, 1992; Tipton and Shoup, 1992).

In this work, numeric simulations with an elastoplastic finite element model are used to estimate the residual stress field present in studless chain links after the proof test and, therefore, before operation. Both constitutive and geometric nonlinearities are considered. A 76 mm studless chain link IACS-W22 Grade 3 is considered (IACS, 1993). The developed analysis considers three material conditions: two associated with limit mechanical properties dictated by IACS-W22 standard and one associated with mechanical properties measured from bars used in the fabrication of the chain link. Results indicate that the presence of residual stresses significantly modifies the stress distribution in the component. Also, residual stress distribution depends on the mechanical properties of the chain link material. The effect of the residual stress on the structural integrity of the chain link is studied using a simplified analysis based on *S-N* curve. This simplified analysis shows that material properties affect the residual stress field, which plays a preponderant part on the structural integrity of chain links.

2. Model

A tridimensional finite element elastoplastic model with large displacements is developed to study the residual stresses in studless chain links. Three planes of symmetry are considered, as shown in Fig. (1a). Numerical simulations are performed with commercial finite element code ANSYS (Ansys, 2001), employing element SOLID95 (20 nodes brick structural solid - 3 degree of freedom per node) for spatial discretization. The final meshes are defined after a convergence analysis. In order to simulate the loading condition, a pressure distribution is applied to the contact area between the chain link and the other mooring elements. This pressure distribution is equivalent to the resultant load in the contact region, and varies linearly from a maximum value to zero at the border of the contact area (Fig. 1b). An angle of 35° with the axial direction (*z* axis) is selected to represent the contact area. Since contact phenomenon is not incorporated into the analysis, it is expected that results near this region are not representative. Nevertheless, results of this model may be useful for the analysis of points far from this region. The geometry of the studless chain link is in accordance with ISO 1704 recommendation (ISO, 1991). For a circular section with diameter *d*, the length is equal to 6*d* and the maximum width is 3.35*d*. In this study the maximum width value is adopted.

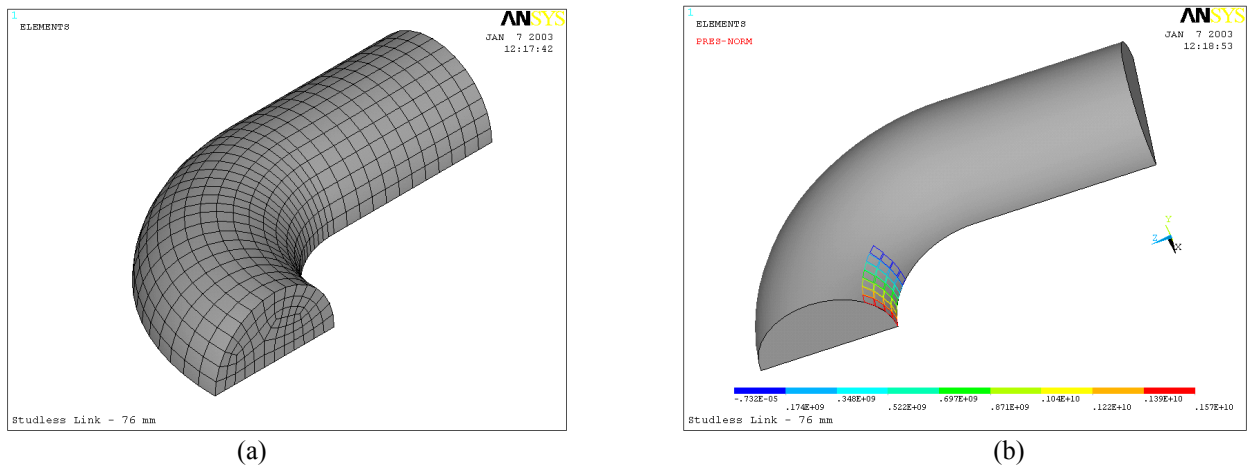<div align="center">(a)   (b)</div>

Figure 1 – Tridimensional finite element model. (a) Mesh and (b) Loading.

In order to estimate the error associated with the application of a pressure distribution over the contact area to simulate the interaction between two chain links, a simplified bidimensional elastoplastic model with contact is developed. This bidimensional model has an equivalent cross section area with a width *d* and a thickness $\pi d/4$. Two planes of symmetry are considered for this situation. Elements PLANE82 (plain strain 8 nodes - 2 degree of freedom per node) are used (Ansys, 2001) for the spatial discretization and the final meshes are defined after a convergence analysis. Figure (2) shows the mesh, load and boundary conditions for two different situations: without and with contact. For the second condition, a one fourth of a second chain link is also included in the model. Contact elements CONTA172 and TARGE169 are used to model the contact between two chain links.
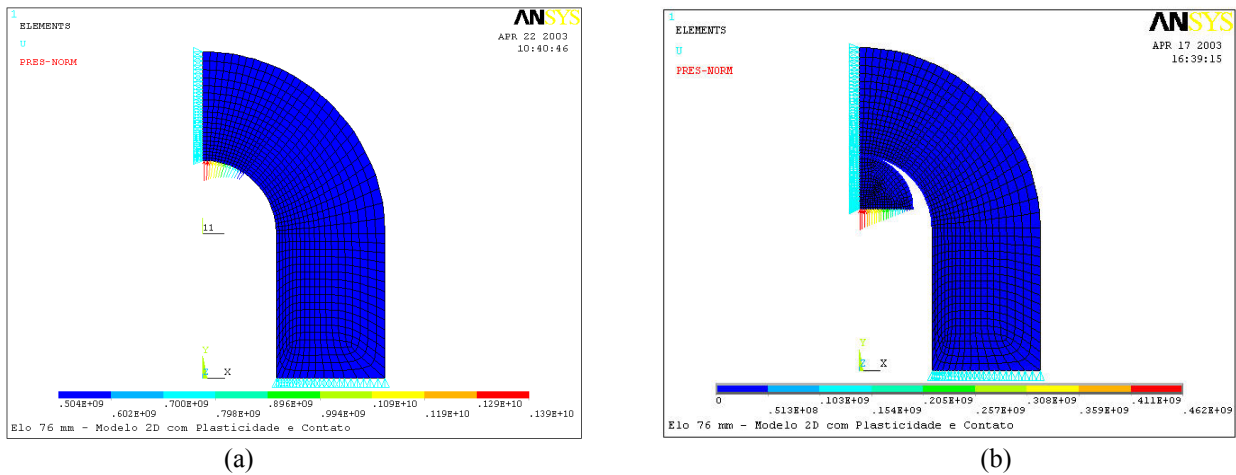
| (a) | (b) |

Figure 2 – Bidimensional finite element model: (a) without contact and (b) with contact.

3.   Numerical Simulations

Numerical simulations are developed to estimate the residual stress distribution in the studless chain links before they enter in operation. The fabrication process of this mechanical component starts with bending and welding of a steel bar at high temperature followed by a heat treatment (quenching and tempering). It is assumed that after this step, the residual stress field is negligible. After this process, a mandatory proof test is applied, promoting a residual stress field on the chain link.

For the numerical simulations presented, a 76 mm studless chain link IACS-W22 Grade 3 is considered (IACS, 1993). The condition prior to operation is achieved by first applying and then removing the recommended proof load, considering an initial material condition prior to the proof test. For the simulations presented, three initial material conditions are considered. The first condition is associated with the minimum mechanical properties dictated by IACS-W22 standard (IACS, 1993) and it is called *IACS-W22$_{Min}$*. The second condition represents a limit material condition for which a ratio between yield and tensile strength of 0.90 is adopted (near IACS-W22 maximum allowable ratio of 0.92), and it is called *IACS-W22$_{0.90}$*. These two conditions furnish a reasonable representation of the material condition range previewed by the standard. The first one represents a material condition with good hardening capability and the second one a material condition with poor hardening capability. The third condition is associated with mechanical properties measured from bars used in the fabrication of the chain link (Petrobras, 2002) and it is called *Measured*. For this condition, the bar was submitted to the quenching and tempering heat treatment dictated by IACS-W22 standard (IACS, 1993). Table (1) presents the mechanical properties adopted for the material condition prior to the proof test.

Table 1 – Mechanical Engineering Properties.

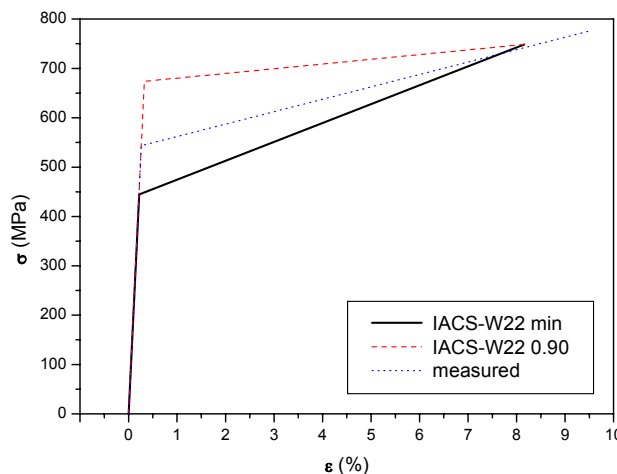|	MATERIAL CONDITION		
Property	*IACS-W22$_{Min}$*	*IACS-W22$_{0.90}$*	*Measured*
Yield Strength - S_y (MPa)	410	621	491
Tensile Strength - S_u (MPa)	690	690	706
Tensile Strength Strain - ε_u (%)	8.5	8.5	10

Figure 3 – Real stress-strain curve for bilinear kinematic hardening model for three material conditions.

An elastic modulus (*E*) of 207 GPa and a Poisson ratio (*ν*) of 0.29 are used in the analysis. For IACS-W22 minimum and 0.90 conditions, the strain associated with the tensile strength (ε_u) is assumed to be half of the total elongation (17%) (IACS, 1993). The engineering stresses and strains listed in Tab. (1) are transformed to real values and used as parameters for a bilinear kinematic hardening model adopted to represent the elastoplastic behavior of the material (Ansys, 2001). Figure (3) shows the real stress-strain curve for the three material conditions used in the bilinear kinematic hardening model. Also, a proof load of 3,242 kN is adopted, according to IACS-W22 (IACS, 1993) for a 76 mm diameter chain link.

Numerical results for the tridimensional model show that extensive plasticity develops in whole component due to the initial proof load. Figure (4) shows the *von Mises* equivalent stress developed during the proof load for the three material conditions. After the load is removed, there are high values of residual stresses of magnitude of the initial yield strength. Figure (5) shows the *von Mises* equivalent residual stress after the proof load for the three material conditions. It can be seen that the initial material condition affects the residual stress distribution. In this work the condition obtained after the application of the proof load is called as *tested*.

It is important to mention that high residual compressive stresses are observed in regions where higher tensile stresses develop during the initial proof load. This effect can be highly beneficial for the fatigue strength of the component as the operational load is lower than the proof load and, therefore, these regions are subjected to lower mean stress component or even with only compressive stresses. For the presented analysis, it is assumed a cyclic load with a maximum value equal to one fourth of the proof load (810 kN) and a minimum value equal to one tenth of the proof load (324 kN). Figure (6) shows the *von Mises* equivalent stress promoted by the application of the maximum operational load in a *tested* chain link. Different behaviors are observed for the three elastoplastic material conditions (Figs. 6*a*-c) that present different critical regions of maximum *von Mises* equivalent stresses. Figure (6*d*) shows the *von Mises* equivalent stress promoted by the application of the operational load considering a fully elastic component. In this case, there are no prior residual stresses, and a completely different stress distribution is obtained when compared with the ones shown in Figs. (6*a*-c). These results suggest that an elastic analysis of the chain links is not sufficient to support a reliable integrity analysis of this type of mechanical component.
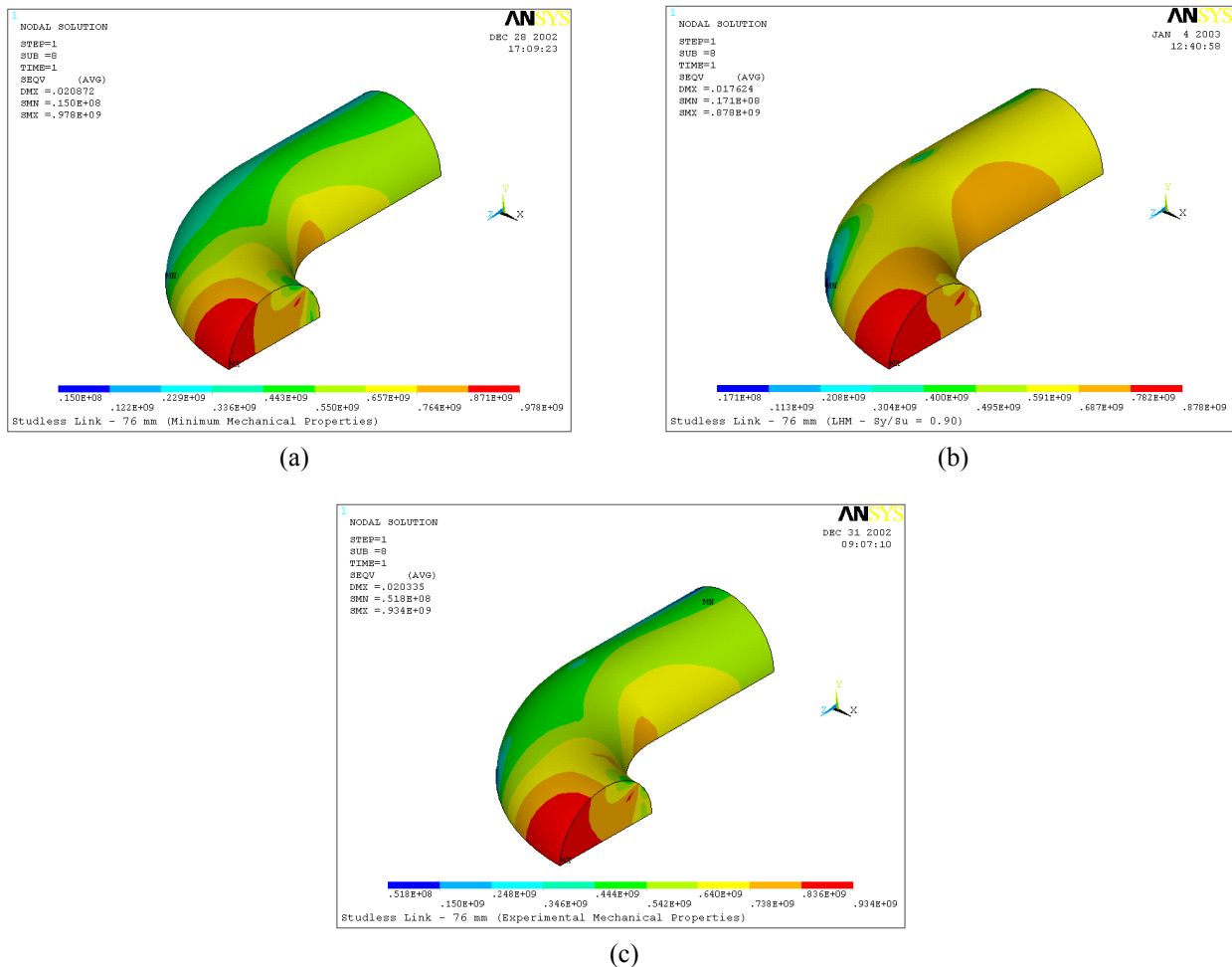

(a)

(b)

(c)

Figure 4 – *von Mises* equivalent stress for the proof test. (a) *IACS-W22$_{Min}$*, (b) *IACS-W22$_{0.90}$* and (c) *Measured* conditions.
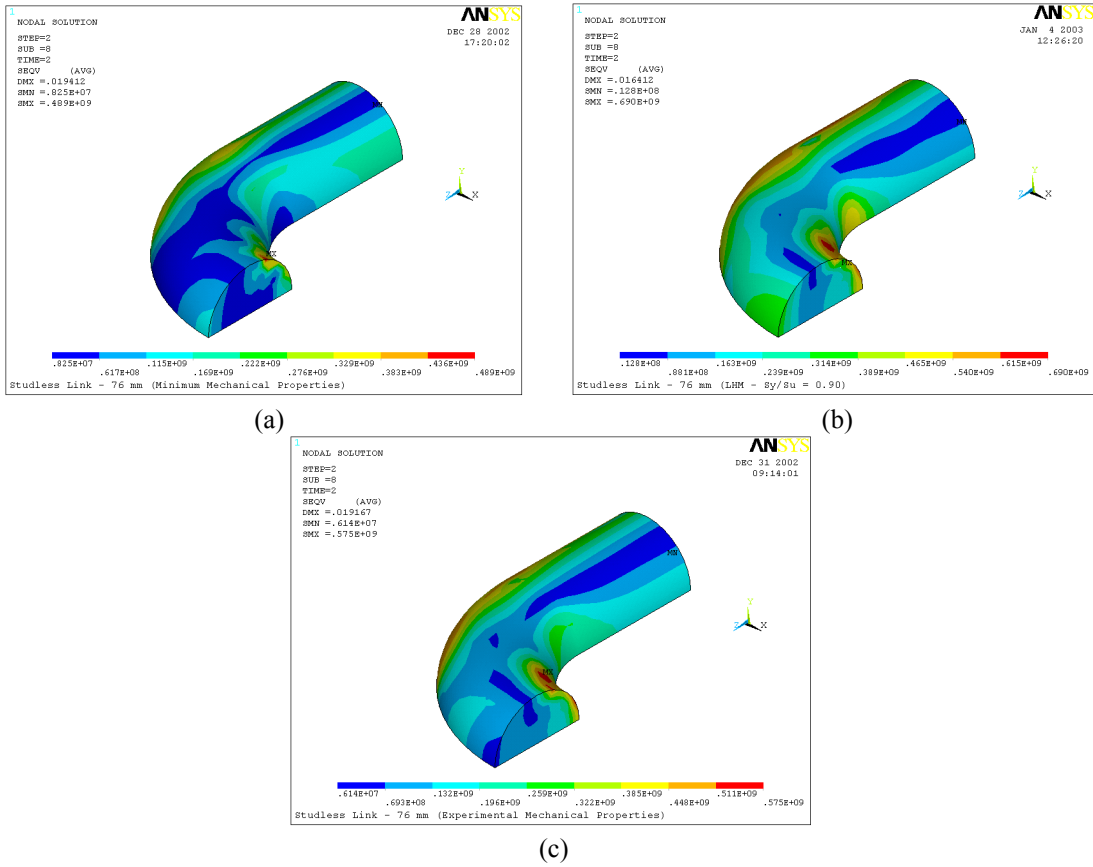
(a)

(b)

(c)

Figure 5 – *von Mises* equivalent residual stress. (a) *IACS-W22$_{Min}$*, (b) *IACS-W22$_{0.90}$* and (c) *Measured* conditions.
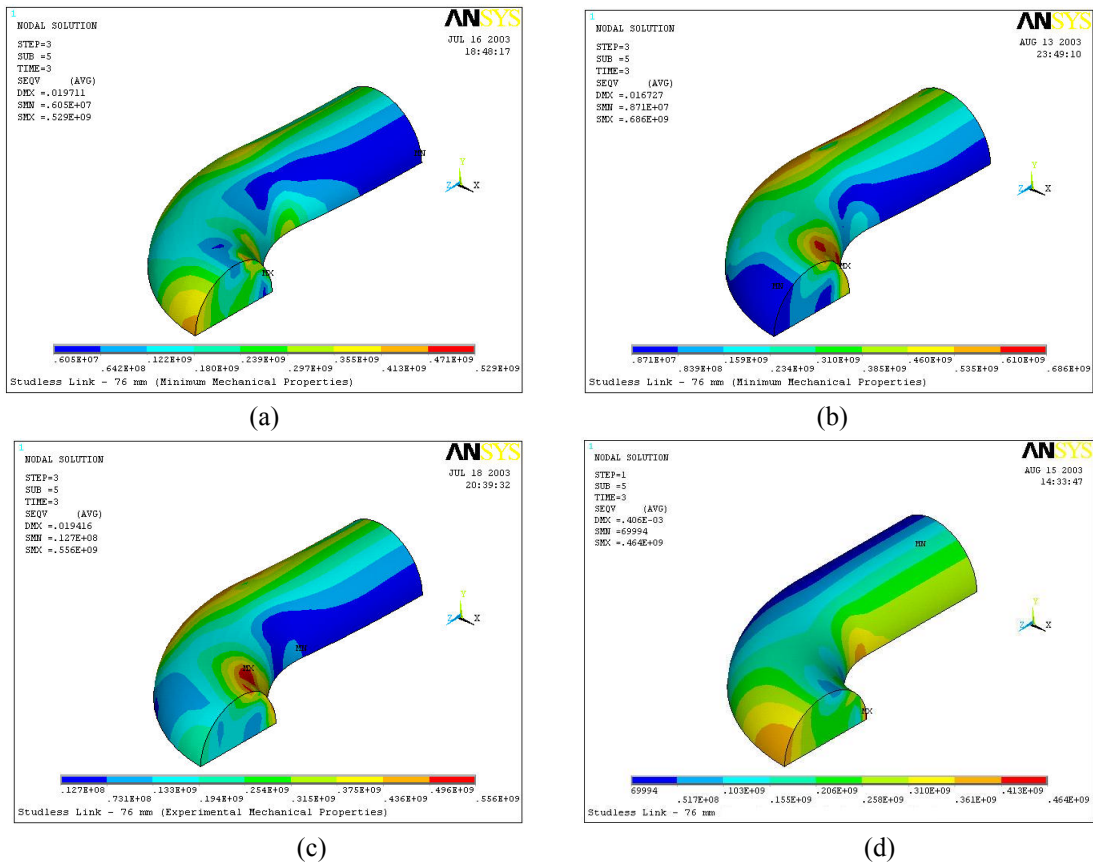

(a)

(b)

(c)

(d)

Figure 6 – *von Mises* equivalent stress for operational loading. Elastoplastic material: (a) *IACS-W22$_{Min}$*, (b) *IACS-W22$_{0.90}$* and (c) *Measured* conditions. Elastic material (d).

The developed stresses are also accomplished in three sections (*A*, *B* and *C*) shown in Fig. (7). The region bonded by red lines represents the region where the pressure distribution is applied. Figures (8-10) shows the longitudinal stress distributions for the three sections analyzed considering the three material conditions plus the elastic material condition. Figure (8) shows the stress distribution for the proof load, Fig. (9) shows the residual stress distribution and Fig. (10) shows the stresses distribution promoted by the operational load. In all these figures, the *Measured* condition lays between the other two, indicating that *IACS-W22$_{Min}$*, and *IACS-W22$_{0.90}$* can be seen as limit cases for the material condition. It is worth to mention that the region near the contact is suppressed in the figures from section *C* since the model does not capture the contact phenomenon that occurs between two chain links, and the results near this region are not representative. The edges length of this suppressed region are approximately two times the edges of the region where the pressure distribution is applied, as shown in Fig. (7) by the region bonded by blue lines.
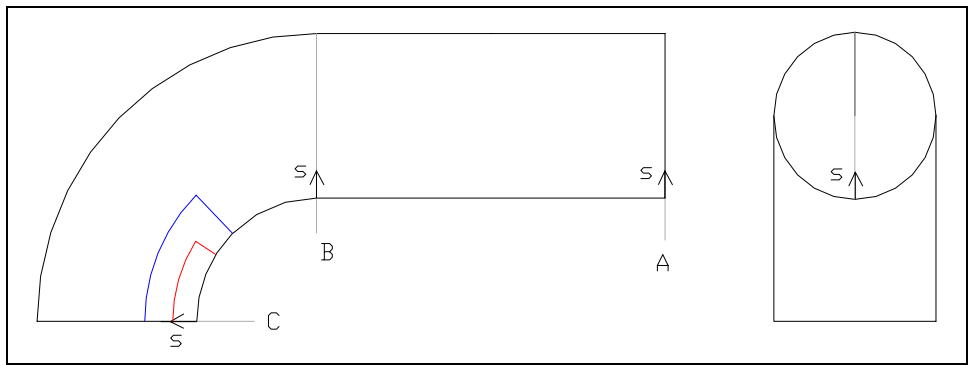

Figure 7 – Sections *A*, *B* and *C*.
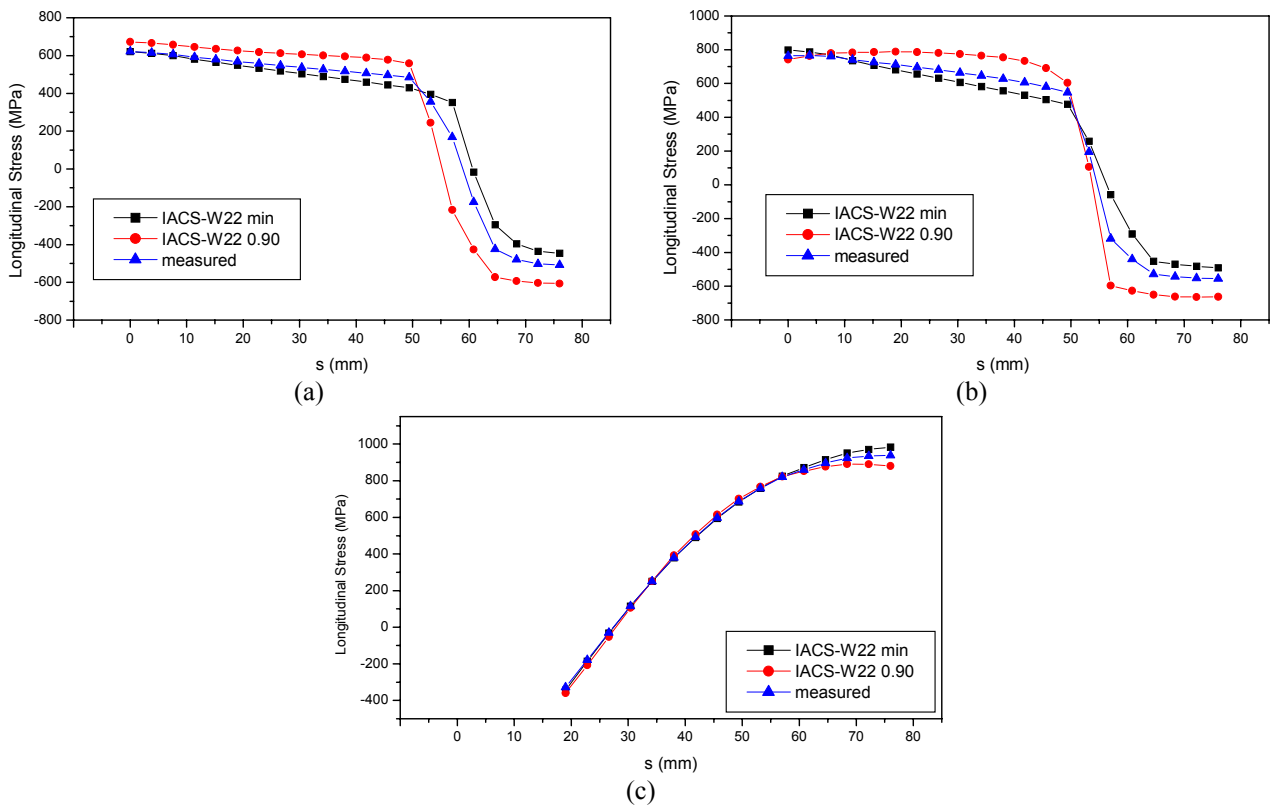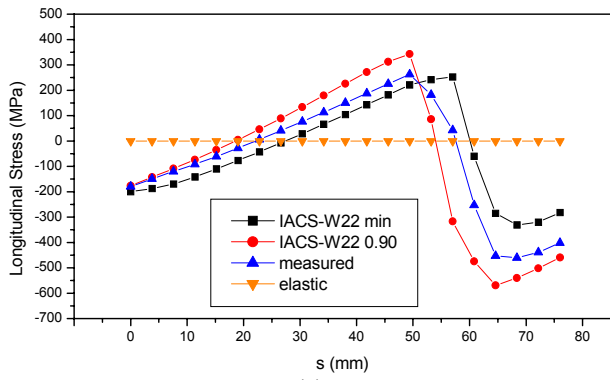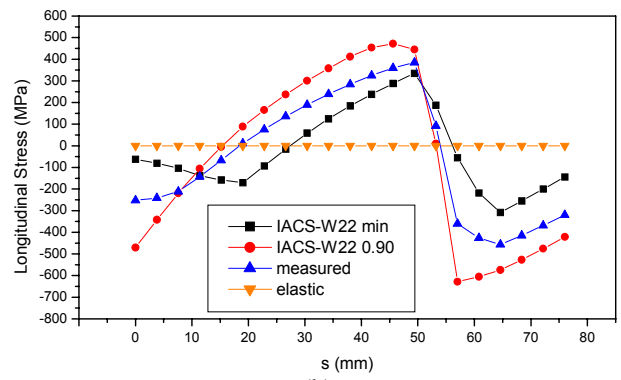

(a)

(b)

(c)
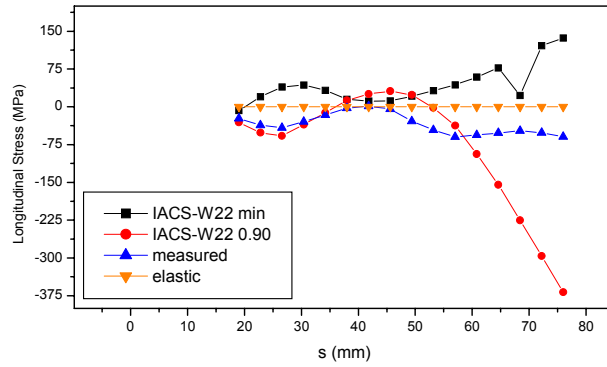
Figure 8 – Longitudinal stress for proof load on sections (a) *A*, (b) *B* and (c) *C*.
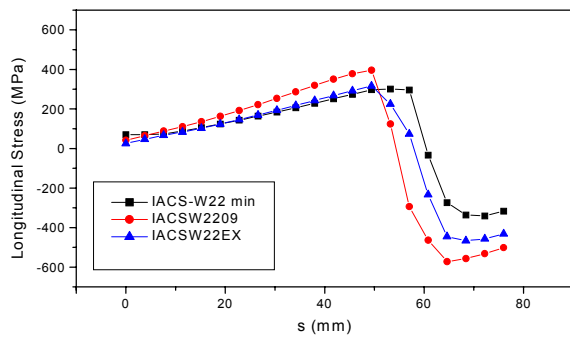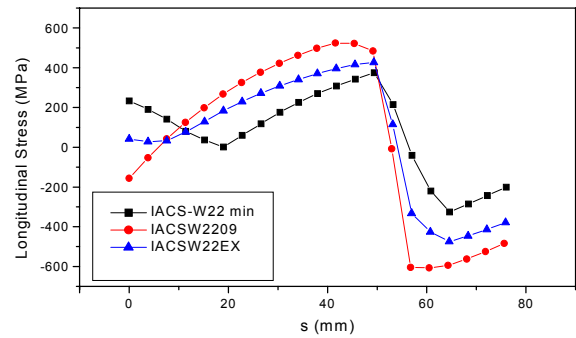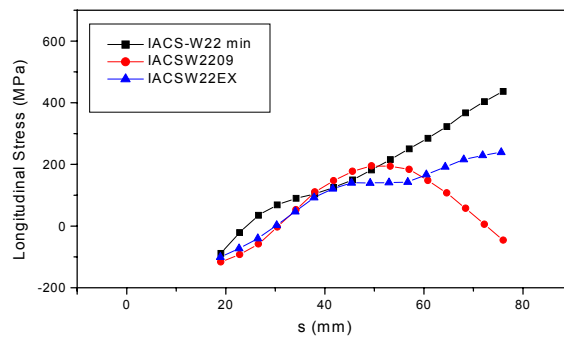
Figure 9 – Longitudinal residual stress on sections (a) *A*, (b) *B* and (c) *C*.

Figure 10 – Longitudinal stress for operational loading on sections (a) *A*, (b) *B* and (c) *C*.

Figure (11) shows the *von Mises* equivalent stress during the proof load and the operational load predicted by the bidimensional model with contact for *IACS-W22$_{Min}$* material condition. Contact angles of 45° and 10° are observed for the proof and operational loads, respectively. It is interesting to note that the contact angle used in the tridimensional analysis (35°) is between these two values.
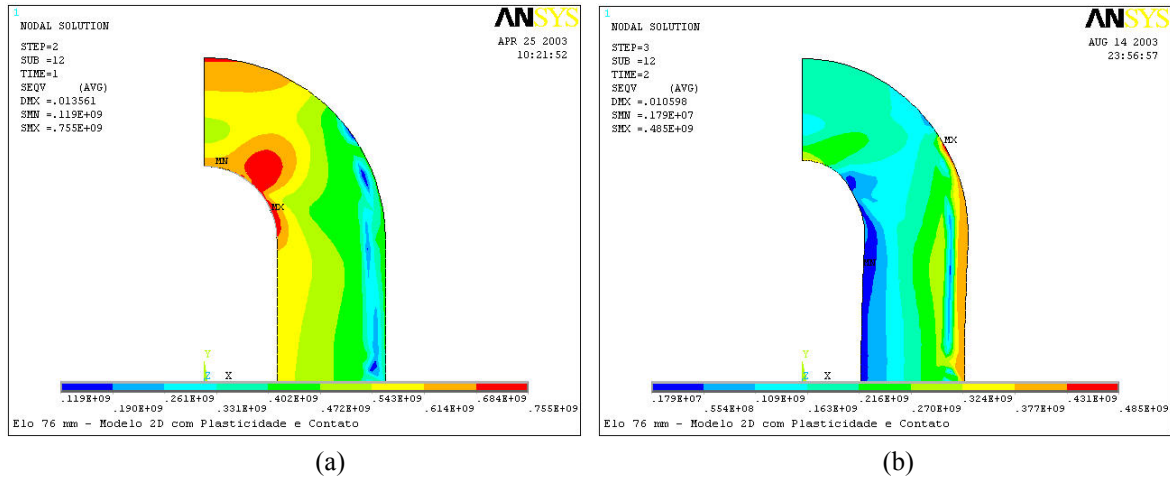

(a)   (b)

Figure 11 – Bidimensional model. *von Mises* equivalent stress for *IACS-W22$_{Min}$*. (a) Proof load and (b) Operational loading.

Figure (12) shows the longitudinal stress distribution during the operational load predicted by the bidimensional model for *IACS-W22$_{Min}$* material condition considering three situations: elastic without contact (2D_E), elastoplastic without contact (2D_EP) and elastoplastic with contact (2D_EPc). Moreover, the elastoplastic tridimensional model for this material condition is presented (3D_EP). A comparison between the tridimensional and bidimensional elastoplastic models without contact shows that the bidimensional model captures the main behavior of the stress distribution. Also, a comparison between the tri-dimensional elastoplastic without contact and bidimensional elastoplastic with contact revels that outside regions near the load application, the two models present a similar behavior. Therefore, this suggests that far from the load application region the stress fields predicted by the tridimensional elastoplastic model (without contact) can be considered representative.
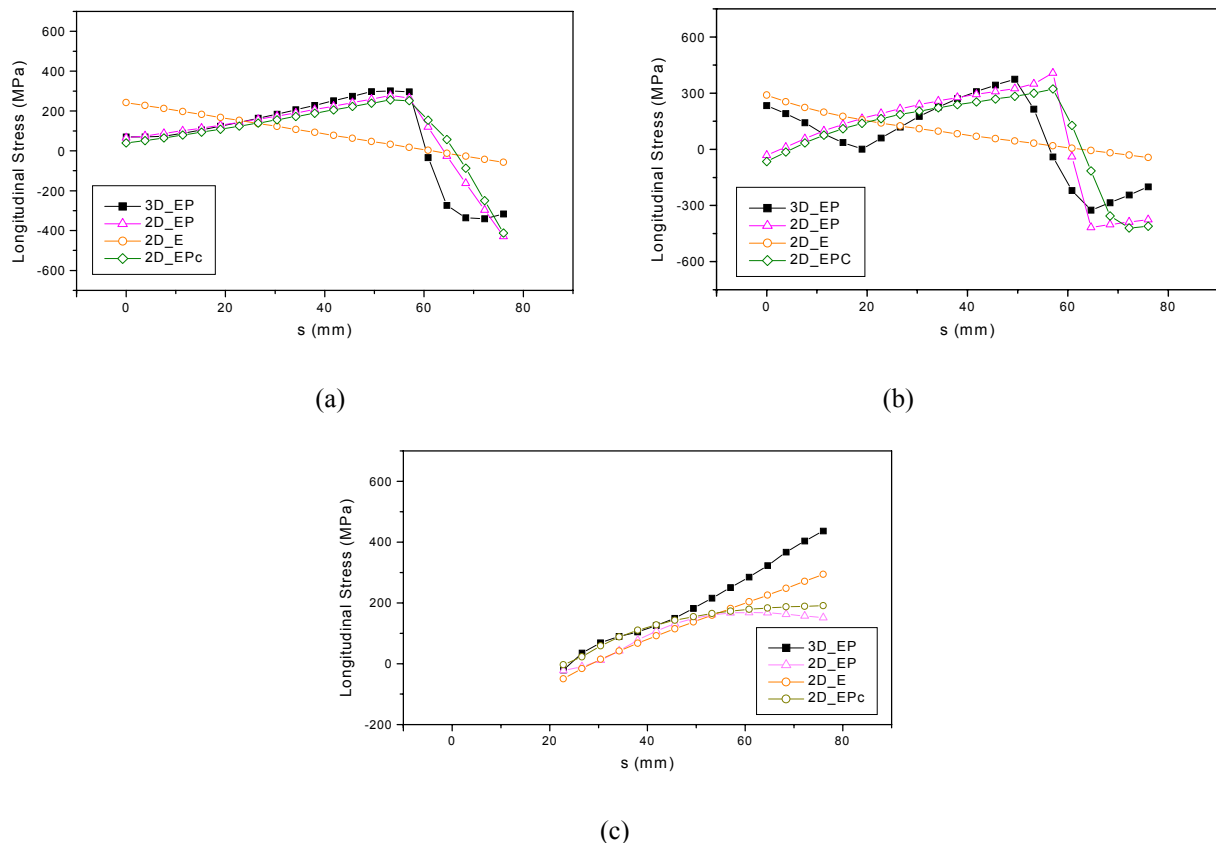

(a)   (b)

(c)

Figure 12 – Bidimensional model for *IACS-W22$_{Min}$*. Longitudinal stress for operational loading on sections (a) *A*, (b) *B* and (c) *C*.

4. Fatigue Life

The API2SK Recommended Practice (API, 1995) furnishes a methodology based on a *T-N* curve (tension *x* number of cycles) that is normally used to predict the fatigue life of mooring line components. This methodology is exclusively based on the load applied on the component and does not consider the stress-state of the component promoted by the applied load. The API2SK furnishes the following *T-N* curve:

$$N R^M = K \tag{1}$$

where *N* is the number of cycles and *R* is the ratio of tension range to nominal breaking strength; *M* and *K* are material parameters. For common chain links, the recommended practice indicates values of 3.36 and 370 for *M* and *K*, respectively (API, 1995).

In this work a value of *R* = 0.10 is adopted which results in a *T-N* fatigue life estimate of 860,000 cycles. In order to perform a direct comparison of the results obtained in the last section, the *S-N* method (with the modified Goodman diagram to consider the mean stress component) is used to estimate the fatigue life of chain links (Shigley and Mischke, 2001). It is assumed that the fatigue life depends on the maximum value of the *von Mises* equivalent stress. Regions near the load application are not considered in the analysis. The border of this region is indicated in Fig. (7) as the region bonded by blue lines. An endurance limit (S_e) of 160 MPa was obtained using the following equation:

$$S_e = k_a \, k_b \, k_c \, k_d \, k_e \, (0.504 \, S_u) \tag{2}$$

and considering the following modification factors: surface factor k_a = 0.52 (hot-rolled), size factor k_b = 0.86 (round bar in bending not rotating), load factor k_c = 1 (bending), temperature factor k_d = 1 (room temperature) and miscellaneous-effects factor k_e = 1 (Shigley and Mischke, 2001). Table (2) presents mean ($\sigma_m^{von\,Mises}$) and amplitude ($\sigma_a^{von\,Mises}$) *von Mises* equivalent stress for the four material conditions (three elastoplastic plus one elastic) in the critical points. The predicted fatigue life (*N*, in cycles) for the four material conditions is presented in Tab. (3) and it is obtained employing the following expressions.

$$N = \left[\frac{\sigma_a^{von\,Mises}}{a} \left(1 - \frac{\sigma_m^{von\,Mises}}{S_u} \right)^{-1} \right]^{1/b} \quad ; \quad a = \frac{(0.9 \, S_u)^2}{S_e} \quad ; \quad b = -(1/3) \log \left(\frac{0.9 \, S_u}{S_e} \right) \tag{3}$$

Table 2 – Fatigue Life Parameters.

MATERIAL CONDITION	Section	*s* (mm)	$\sigma_m^{von\,Mises}$ (MPa)	$\sigma_a^{von\,Mises}$ (MPa)
IACS-W22$_{min}$	C	76	337	93
IACS-W22$_{090}$	C	76	142	96
Measured	C	76	156	87
Elastic	C	76	182	182

Table 3 – Predicted Fatigue Life.

MATERIAL CONDITION	N (thousands of cycles)
IACS-W22$_{min}$	502
IACS-W22$_{090}$	3,988
Measured	5,873
Elastic	106

It should be pointed out that the *T-N* curve methodology predicts an intermediary value between the ones predicted by the proposed methodology using the elastoplastic model. As expected, the elastic model presents the smaller fatigue life as it predicts higher levels of maximum stresses suggesting that elastic model is conservative when compared to elastoplastic models. Elastoplastic models present a very distinct behavior confirming that fatigue life is strongly dependent on the material condition.

5. Conclusions

This work presents a study on the effect on the material condition of residual stresses and structural integrity of studless chain links with respect to their fatigue life. Three material conditions are considered in order to analyze the effect of material properties on residual stress distribution. A tridimensional finite element elastoplastic model is developed in order to estimate the residual stress distribution before operation for 76 mm studless chain links. Numerical simulations show that there are high values of residual stresses (of the initial yield strength magnitude) before the chain link enters in operation. For a typical operational loading condition, numerical simulations show that the elastoplastic analysis furnishes a completely different stress distribution than the one obtained in an elastic analysis, due to the high level of residual stresses in a chain link. These results suggest that an elastic analysis of the chain links is not sufficient to support a reliable integrity analysis of this type of mechanical component. Also, the residual stress field developed after the proof tests depends on the material condition. A simplified *S-N* method is used to estimate the fatigue life of the chain links in a comparative study using results obtained in the numerical simulations for the three material conditions. Results show that the material condition significantly influences the residual stress developed and have a preponderant effect on the structural integrity of chain links. It's worth to mention that important effects, like the contact phenomenon that occurs between two chain links, must be addressed in a more detailed analysis using a tridimensional model in future works. Moreover, an experimental program to measure residual and operational stresses must be established.

6. Acknowledgements

7. References

Almer, J.D., Cohen, J.B. and Moran, B., 2000, "The Effects of Residual Macrostresses and Microstresses on Fatigue Crack Initiation", *Materials Science and Engineering*, A284**,** pp. 268–279.

Ansys, 2001, "Ansys Manual", Release 5.7, Ansys Inc.

API – American Petroleum Institute, 1995, "*Recommended Pratice for Design and Analysis of Stationkeeping Systems for Floating Structures*", API Recommended Practice 2SK.

Chaplin, C.R., Rebel G., and Ridge, I.M.L., 2000, "Tension/Torsion Interactions in Multicomponent Mooring Lines", *Proceedings of the 2000 Offshore Technology Conference – OTC2000*, paper OTC 12173.

Hasson, D.F., and Crowe, C.R., 1988, "*Materials for Marine Systems and Structures*", Treatise on Materials Science and Technology, Vol.28, Academic Press.

IACS**,** 1993, "Unified IACS Requirements Concerning Materials and Welding – W22 Offshore Mooring Chain", International Association of Classification Societies.

ISO, 1991, "*ISO 1704 - Shipbuilding stud-link anchor chains*", 2nd Edition, International Organization for Standardization.

Pacheco, P.M.C.L.; Kenedi, P.P. and Jorge, J.C.F., 2002, "Elastoplastic Analysis of the Residual Stress in Chain Links", *OMAE'2002 - 21st International Conference on Offshore Mechanics and Arctic Engineering*, Oslo, Norway.

Paiva, A.M.C., 2000, "*Mooring Systems Integrity: Contributions to Metodology Analysis*" (in Portuguese), Master Degree Thesis, Department of Mechanical Engineering CEFET/RJ.

Papazoglou, V.J., Katsaounis, G.M., and Papaioannou, J.D., 1991, "Elastic Analysis of Chain Links in Tension and Bending", *Proceedings of the First International Offshore and Polar Engineering Conference*, Edinburgh, U.K., Vol. II, pp. 252-258.

Petrobras, 2002, "*Internal Report*", Petrobras.

SAE, 1988, *"Fatigue Design Handbook"*, SAE – Society of Automotive Engineers.

Shigley, J.E. and Mischke, C.R., 2001, *"Mechanical Engineering Design"*, 6th edition, McGraw-Hill.

Shoup G.J., Tipton S.M. and Sorem Jr., 1992, "The Effect of Proof Loading on the Fatigue Behavior of Stud Link Chain" *International Journal of Fatigue*, No.14 (1), pp.35-40.

Stern, I.L., and Weatcroft, M.F., 1978, "Towards Improving the Reliability of Anchor Chain and Accessories", *Proceedings of the 1978 Offshore Technology Conference – OTC1978*, paper OTC 3206.

Tipton S.M. and Shoup G.J., 1992, "The Effect of Proof Loading on the Fatigue Behavior of Open Link Chain", *Journal of Engineering Materials and Technology-Transactions of the ASME*, No.114 (1), pp. 27-33.

Webster, G.A. and Ezeilo, A.N., 2001, "Residual Stress Distributions and their Influence on Fatigue Lifetimes", *International Journal of Fatigue*, 23**,** pp. S375–S383.

8. Copyright Notice